

Core-Collapse Simulations of Rotating Stars

Chris L. Fryer & Alexander Heger
Lick Observatory, University of California Observatories,
Santa Cruz, CA 95064
cfryer@ucolick.org, alex@ucolick.org

ABSTRACT

We present the results from a series of two-dimensional core-collapse simulations using a rotating progenitor star. We find that the convection in these simulations is less vigorous because a) rotation weakens the core bounce which seeds the neutrino-driven convection and b) the angular momentum profile in the rotating core stabilizes against convection. The limited convection leads to explosions which occur later and are weaker than the explosions produced from the collapse of non-rotating cores. However, because the convection is constrained to the polar regions, when the explosion occurs, it is stronger along the polar axis. This asymmetric explosion can explain the polarization measurements of core-collapse supernovae. These asymmetries also provide a natural mechanism to mix the products of nucleosynthesis out into the helium and hydrogen layers of the star. We also discuss the role the collapse of these rotating stars play on the generation of magnetic fields and neutron star kicks. Given a range of progenitor rotation periods, we predict a range of supernova energies for the same progenitor mass. The critical mass for black hole formation also depends upon the rotation speed of the progenitor.

Subject headings: black hole physics - stars: rotation - supernova: general

1. Introduction

The study of the collapse of *rotating* massive stars is nearly as old as the study of core-collapse supernovae themselves. Four years after the first numerical simulations of neutrino powered core-collapse supernovae (Colgate & White 1966), LeBlanc & Wilson (1970) modeled the core-collapse of a rotating massive star. Instead of using neutrinos to convert gravitational energy into kinetic energy and power the explosion (Colgate & White 1966), LeBlanc & Wilson (1970) proposed that supernovae were powered by the conversion of rotational energy using magnetic fields. Although neutrino heating is now considered to be the dominant power source driving supernovae, the importance of rotation remains a matter of dispute.

Most of the recent work studying the collapse of rotating massive stars has concentrated on the emission of gravitational waves (Müller, Różyczka, & Hillebrandt 1980; Tohline, Schombert, & Boss 1980; Finn & Evans 1990; Mönchmeyer et al. 1991; Bonazzola & Marck 1993; Yamada & Sato 1995; Zwerger & Müller 1997; Rampp, Müller, & Ruffert 1998). Some of the work, however, was devoted to understanding

the effect of rotation upon the supernova explosion itself (Müller & Hillebrandt 1981; Bodenheimer & Woosley 1983; Symbalisty 1984; Mönchmeyer & Müller 1989; Janka & Mönchmeyer 1989; Janka, Zwerger, & Mönchmeyer 1993; Yamada & Sato 1994). Currently, no consensus on the effects of rotation has been reached. For instance, there is still disagreement on whether rotation increases or decreases the explosion energy. Mönchmeyer & Müller (1989) found that rotation weakens the core bounce, ultimately weakening the explosion. On the other hand, the asymmetry in the neutrino emission caused by rotation may help seed convection, increasing the efficiency of neutrino heating and ultimately producing a more powerful explosion (Yamada & Sato 1994).

The simplifying assumptions in all of these simulations make it difficult to resolve this disagreement. For instance, none of the above simulations incorporated neutrino transport into their multi-dimensional hydrodynamic simulations. Many of the simulations use extremely simplified equations of state which, as Müller & Hillebrandt (1981) discovered, alters significantly the effect of rotation. In addition, the pre-collapse cores used in these models were all created assuming no rotation, and the angular momentum was then added artificially prior to the collapse simulation.

Two major advances in supernova theory seek to resolve the question of rotation effects on core-collapse. First, in the past 5 years, codes have been developed with the necessary equations of state and neutrino physics to model the core collapse in two-dimensions from the initial collapse all the way through explosion (Herant et al. 1994; Burrows, Hayes, & Fryxell 1995, Fryer 1999). In addition to improvements on the collapse codes, Heger (1998); Heger, Langer, & Weaver (1999), has evolved rotating massive stars to core-collapse using a prescription for the transport of angular momentum, producing rotating core-collapse progenitors. In this paper, we present results of collapse simulations of these rotating massive cores.

In §2, we outline the assumptions of the progenitor models and discuss the specific progenitor we use in our simulations. The core collapse code is described in §3 and the basic effects of rotation are outlined in §4. We find that not only is the bounce of rotating stars weaker, but the angular momentum in the star stabilizes the core, constraining convection to the poles. These two effects decrease dramatically the efficiency at which convection is able to convert neutrino energy into kinetic energy. The net effect is to delay the supernova explosion, producing larger compact remnants and weaker explosions. We present the explosion simulations for all our models in §5. The asymmetry in the convection produces asymmetric explosions which may explain polarization measurements of supernovae and may inject alpha-elements deep into the star’s envelope. We conclude by reviewing the implications of these results on core-collapse supernovae, black hole formation, and the collapsar gamma-ray burst model.

2. Progenitor

All of the previous collapse simulations of rotating cores prescribed an angular momentum profile onto a non-rotating progenitor. For our simulations, we use the $15 M_{\odot}$ rotating progenitor E15B of Heger et al. (1999). At central hydrogen ignition, this model has a “solar” composition (Grevese & Noels 1993) and an equatorial rotation velocity of 200 km s^{-1} which is a typical value for these stars (e.g., Fukuda 1982). For this model, redistribution of angular momentum and chemical mixing was formulated similar to the technique of Endal & Sophia (1978) and used a parameterization of the different mixing efficiencies similar to that of Pinsonneault et al. (1989). The rotationally induced mixing processes include dynamical and secular shear instability, Solberg-Høiland instability, Goldreich-Schubert-Fricke instability, and Eddington-Sweet circulation. All these mixing processes, as well as the convective instability, were assumed to lead to

rigid rotation on their corresponding time-scale (Fig. 1 shows the evolution of the angular momentum at various stages of the star’s life). Equipotential surfaces were assumed to be rigidly rotation and chemically homogeneous due to the barotropic instability and horizontal turbulence (Zahn 1975; Chaboyer & Zahn 1992; Zahn 1992). Magnetic fields were not considered, since their efficiency in redistributing angular momentum (and mixing) inside stars is still very controversial (e.g., Spruit & Phinney 1998, Spruit 1998 vs. Livio & Pringle 1998) and no reliable prescriptions exist yet. For more detail on the progenitor model and the input physics we refer the reader to Heger (1998); Heger et al. (1999).

If magnetic fields are strong, the angular velocity between the core and surface may couple during most evolutionary phase, leading to much smaller core rotation rates than found by Heger et al. (1999). In the model for the evolution of an internal stellar magnetic field by Spruit & Phinney (1998), the core rotation decouples from the surface only *after* central carbon depletion. The cores resulting from their calculation carry far too little angular momentum to explain the observed rotation rates of young pulsars (Marshall et al. 1998), and thus Spruit & Phinney (1998) have to employ another mechanism to spin them up again. Livio & Pringle (1998) instead find that the coupling between core and envelope due to magnetic fields should be far less than assumed by Spruit & Phinney (1998), allowing a natural explanation for spin rates of both young pulsars and white dwarfs.

With regard to the relevant physics in core-collapse and the neutrino-driven supernova mechanism, the structure of our rotating progenitor is not too different from that of Woosley & Weaver (1995). Figure 2 shows the density and temperature profiles just before collapse for our rotating progenitor and model s15s7b from Woosley & Weaver (1995). Note that beyond a radius of $\sim 3 \times 10^8$ cm, the density of the non-rotating star is roughly a factor of 2 lower than that of the non-rotating Woosley & Weaver progenitor. Pressure equilibrium requires that the temperature at these radii also be lower. Burrows & Goshy (1993) have shown that cores with lower densities are more likely to explode because the ram pressure which prevents the explosion is lower for these cores (see §4). However, the differences between these two stars are small enough that they do not change the ultimate features in the core-collapse significantly (§5).

The angular momentum distribution, on the other hand, does dramatically effect the collapse. The angular velocity profile of our rotating progenitor is shown in Figure 3. For comparison, we have included the angular velocity profiles of many of the models used by Mönchmeyer & Müller (1989). Rather than use a rotating progenitor, Mönchmeyer & Müller (1989) added these angular velocities onto a non-rotating progenitor. Their model A closely resembles our rotating progenitor, but most of their models have higher angular velocities, and the effects of rotation are stronger for most of their simulations. In addition, our angular velocity distribution consists of a series of discreet shells which rotate at constant angular velocity whereas the Mönchmeyer & Müller (1989) models all assume a continuous rotation distribution. These discreet shells are the result of discreet convection regions in the progenitor star. The strong convection in the star causes the material in each shell to reach a constant angular velocity (rigid body rotation). However, shear viscosity does not equilibrate adjacent shells and, at the boundaries of convective regions, the angular velocity can change abruptly. The evolution of the core collapse depends most sensitively on the magnitude of the rotation speed and not its derivative and, hence, the initial collapse of model A from Mönchmeyer & Müller (1989) agrees well with our simulations (see §4).

3. Numerical Techniques

For our simulations, we use the smooth particle hydrodynamics (SPH) core-collapse code originally described in Herant et al. (1994) and Fryer et al. (1999). This code models the core collapse in two dimensions continuously from collapse through bounce and ultimately to explosion. The neutrino transport is mediated by a single energy flux-limiter. Beyond a critical radius, $\tau < 0.1$, a simple “light-bulb” approximation for the neutrinos is invoked which assumes that any material beyond that radius is bathed by an isotropic flux equal to the neutrino flux escaping that radius. We use all the neutrino production and destruction processes discussed in Herant et al. (1994) *except* electron scattering because our neutrino transport algorithm overestimates its effect. We implement gravity assuming the mass distribution is spherical. Assuming a spherical mass distribution also allows us to easily implement general relativity fully into the equations of motion using the technique described by Van Riper (1979). This treatment includes both the relativistic modifications to the energy equation and time dilation. We further red-shift the neutrino energies as the neutrinos climb out of the core’s potential well.

Our two-dimensional simulations assume cylindrical symmetry about the rotation axis, modeling a full 180° wedge with a reflective boundary around the symmetry axis. The inner $0.01M_\odot$ is also modeled as a reflective boundary which collapses along with the star as described in Herant et al. (1994). Because the progenitor models did not account for centrifugal acceleration, we had to artificially add $0.04M_\odot$ to the inner core to induce a collapse (hence, the inner core has an effective mass of $0.05M_\odot$). We also ran a set of simulations with an additional $0.04M_\odot$ to the core but the results did not change (Table 2). For most of our simulations, we use ~ 9000 particles with a resolution in the convection parts of the star of roughly 2° . We have run one model with $\sim 32,000$ particles (twice the resolution) and the results do not change significantly (Table 2).

The initial angular momentum distribution of the progenitor (See §2; Heger et al. 1999) is mapped onto the 2-dimensional grid of particles assuming that the rotation axis is identical to the symmetry axis. Each particle is given an initial specific angular momentum: $j_i = (x_i/r_i)j(r)$ where r_i , x_i are the radial distance and the particle distance from the rotation axis and $j(r)$ is the angular momentum given by E15B progenitor of Heger et al. (1999; Fig. 3). We have also set up models using $j_i = 0.5(x_i/r_i)j(r)$ and $j_i = 0$. For most of our simulations, we assume that the angular momentum is conserved, which in our 2-dimensional SPH code is true simply by holding j_i constant for each particle. The force on the particles, which are rings in our rotationally symmetric simulation, is modified by adding the centrifugal force: $\equiv j_i^2/x_i^3$. By ranging the initial angular momenta of the particles, we can calculate the effects of rotation.

However, in our rotating models, the angular velocity of the matter (v^ϕ) becomes so high that it may rotate 10-100 periods ($P_i = 2\pi x_i/v_i^\phi$) during the course of the ~ 1 s simulation. In this case, it is likely that viscous forces will facilitate the transport of angular momentum. To estimate the effects of these viscous forces, we have implemented an α -disk viscosity (Shakura & Sunyaev 1973) which is suitable for the disk-like structures that develop as the core collapses. We use the shear viscosity tensor from Tassoul (1978) and drop the terms involving a derivative in ϕ (since $\partial X/\partial\phi = 0$ in our rotational symmetry). Using our SPH formalism, the transport of angular momentum is:

$$\frac{Dj_i}{Dt} = \sum_k \alpha_d \bar{c}_s \bar{H}_p \bar{x} \frac{\bar{m}}{m_i} \left[\frac{3\Delta(v^\phi/x)}{r_{ik} + \epsilon\bar{h}} + \frac{\bar{x}\Delta(v^\phi/x)}{r_{ik}^2 + \epsilon\bar{h}^2} + \frac{\bar{x}\Delta(v^\phi)}{r_{ik} + \epsilon\bar{h}} \right] \quad (1)$$

where $\alpha_d = 0.1 - 10^{-4}$ is the α -disk parameter, \bar{c}_s , \bar{H}_p , \bar{x} , \bar{m} , and \bar{h} are the mean values between neighbor particle i and k of, respectively, the adiabatic sound speed, the disk scale height, the distance from the rotation axis, the particle mass, and the SPH smoothing length. $\Delta(v^\phi/x) = (v_i^\phi/x_i - v_k^\phi/x_k)$,

$\Delta(v^\phi) = (v_i^\phi - v_k^\phi)$, r_{ik} is the separation of particles i and k and $\epsilon = 0.1$. The net energy lost by the particles is then added to the particles equally as dissipation energy which is equivalent to using the dissipation function given in Tassoul (1978). The summation occurs over all of the SPH neighbors of particles for which $P_i < 1$ s. This implementation conserves angular momentum and energy and the α -disk viscosity gives some insight into the effects of viscous forces.

To follow the progression of the supernova explosion to late times (~ 1 yr after core collapse), we convert from our 2-dimensional results back into the one-dimensional stellar evolution code KEPLER (Weaver, Zimmermann, & Woosley 1978). This is the same code that has been used to evolve the stars until core collapse (Heger 1998; Heger, Langer, & Woosley 1999). Unfortunately, KEPLER simulates the explosion using a “piston” rather than a simple injection of energy which matches the physics more reliably. The piston moves inward at free-fall until then infall velocity reaches about $1,000 \text{ km s}^{-1}$ at which point it bounces and moves outward until it reaches a final position of 10^4 km. The first part of the piston movement is taken from the SPH simulation by following the trajectory of a spherical mass shell. This method leads to a systematic underestimate of the energy input, because any spherically determined mass shell has matter flowing through it and although the mean velocities of the exploding matter is matched by the spherically determined mass trajectories, total energy in the explosion can be much higher. As the simulation progresses beyond the maximum time from our two-dimensional simulations, we continue the movement of the piston such that it resembles the free movement of a test particle in the gravitational field of a point mass equal to α times the mass interior to the piston which reaches zero velocity at the final location of the piston (10^4 km; see above), following the prescription by Woosley & Weaver (1995).

The value of α is chosen such that it “smoothly” continues the piston movements obtained from the SPH simulations. This, however, involves some ambiguity (about a factor of two in α , we estimate), since we have no measure to quantify the quality of this fit. The values of α we use are given in Table 3. We carry out these extended SN simulations for a rotating model (Model 1; see Table 1) and a non-rotating model (Model 6) and for different locations, in mass, of the piston (Table 3). For Model 6 we switch to the “artificial” piston after 1.9 s after the onset of core collapse, for Model 6 after 1.0 s. The contribution of this artificial continuation of the SPH-derived pistons to the total work of the piston is also given in Table 3: in most cases it is only small and thus our choice of α should not significantly alter our results. We note that during the inward movement of the piston a work of about 10^{51} erg (for Model 1, $1.1 M_\odot$ piston) is done against the piston by the infall and thus the work of the piston counting from its minimum location (in radius) is higher by this amount. The piston energies given in Table 3 are the integrated work energies from the beginning of the SPH simulation till ~ 1 yr after the core collapse.

For the non-rotating Model 6 we also carry out a series of explosions where we start the “artificial” piston at the minimum location of the piston (as obtained from the SPH simulation) at a mass coordinate of $1.1 M_\odot$ and for different values of α . In comparison to the model of same mass cut but using the artificial piston only after the end of the SPH data we get the same energies within less than 1%. The explosion energy turns out to be rather insensitive to the value of α . Due to the above-mentioned underestimate of the explosion energy in the 1D simulation, a more than six times higher value of α ($\sqrt{6}$ times higher piston velocity) is necessary to obtain the same explosion energy than in the SPH simulation. By using the results from this series of piston simulations, we can estimate not only the kinetic energies of our supernova explosions, but also the amount of fallback and ^{56}Ni ejected (Table 2).

4. Collapse and Convection

The evolutionary scenario for the current paradigm of core-collapse supernovae begins with the collapse of a massive star ($M_{\text{star}} \gtrsim 8 M_{\odot}$) which occurs when the densities and temperatures at the core are sufficiently high to cause both the dissociation of the iron core (removing energy from the core) and the capture of electrons onto protons which further reduces the pressure. This sudden decrease in pressure causes the core to collapse nearly at free-fall, and the collapse stops only when nuclear densities are reached and nucleon degeneracy pressure once again stabilizes the core and drives a bounce shock back out through the core. The bounce shock stalls at roughly 100-300 km as neutrino emission and iron dissociation sap its energy. It leaves behind an entropy profile which is unstable to convection, and sets up a convective region from ~ 50 km out to ~ 300 km (Fig. 4) capped by the accretion shock of infalling material. The convective region must overcome this cap to launch a supernova explosion.

Neutrino heating deposits considerable energy into the bottom layers of the convective region. If this material were not allowed to convect (which is the case for most of the 1-dimensional simulations), it would then re-emit this energy via neutrinos producing a steady state with no net energy gain. In the meantime, the increase in pressure as more material piles up at the accretion shock and the decrease in neutrino luminosity as the proto-neutron star cools make it increasingly difficult to launch an explosion. In the “delayed-neutrino” supernova mechanism (Wilson & Mayle 1988; Miller, Wilson, & Mayle 1993; Herant et al. 1994; Burrows, Hayes, & Fryxell 1995; Janka & Müller 1996), convection aids the explosion in two ways: a) as the lower layers of the convective region are heated, that material rises and cools adiabatically and converts the energy from neutrino deposition into kinetic and potential energy rather than re-radiating it as neutrinos, and b) the material does not simply pile at the shock but instead convects down to the surface of the proto-neutron star where it either accretes onto the proto-neutron star providing additional neutrino emission or is heated and rises back up. Thus, convection both increases the efficiency at which neutrino energy is deposited into the convective region and reduces the energy required to launch an explosion by reducing the pressure at the accretion shock. It appears that nature has conspired to make core-collapse supernovae straddle the line between success and failure, where convection, which for years was thought to be a mere detail, plays a crucial role in the explosion. It is not surprising that the outcome of the core collapse of massive stars depends upon numerical approximations of the physics, for example, the algorithm for neutrino transport (Messer et al. 1998; Mezzacappa et al. 1998a). It is also not surprising that changes in the progenitor, i.e. the subject of this paper, rotation, also can lead to different outcomes.

For a rotating core-collapse, this basic evolutionary history remains the same, but many aspects of the collapse, bounce, convection, and explosion phases change. To determine these variations, we compare a rotating star (E15B from Heger et al. 1999) with its non-rotating counterpart (Unless otherwise stated, all quantitative results and figures compare Models 1 and 6). First, angular momentum slows the collapse and delays the bounce (Mönchmeyer & Müller 1989; Janka & Mönchmeyer 1989). For our rotating model, the bounce occurred 200 ms into the simulation, a full 50 ms longer than the non-rotating counterpart. For very high angular momenta, the central density at bounce can be lower than a non-rotating star by over an order of magnitude (Mönchmeyer & Müller 1989; Janka & Mönchmeyer 1989), but for the more modest angular momenta from Heger et al. (1999), the central density at bounce drops from $4 \times 10^{14} \text{ g cm}^{-3}$ for a non-rotating star to $3 \times 10^{14} \text{ g cm}^{-3}$ for the rotating case. This lower critical bounce density occurs because the centrifugal force begins to provide significant support (it increases from 2% to 10% that of the gravitational force over the course of the simulation). The resulting bounce shock is weaker and, along the poles, stalls at lower radii than the non-rotating case. Along the equator where the effective gravity is less, the accretion shock moves much further, and the star quickly loses its spherical symmetry (Fig.

5). 60 ms after the bounce, the accretion shock of the rotating model is at $\sim 160, 300$ km respectively for the poles, equator. At that time, the spherically symmetric accretion shock of the non-rotating star is at ~ 300 km.

The position of the accretion shock, initially set by the position at which the bounce stalls, is important for the success or failure of the convection-driven supernova mechanism because it determines the ram pressure that the convective region must overcome to drive an explosion. Even more important, however, is the entropy profile that is left behind after the bounce fails. Because the bounce is weaker for rotating stars, the angle-averaged entropy decreases with increasing angular momentum (Fig. 6). The entropy in the strong shock limit is $\propto v_{\text{shock}}^{1.5}$, and along the equator, where the material is collapsing less quickly, the entropy is much lower (Fig. 7). The steep entropy gradient in supernovae is what seeds the convection and the shallower gradients in the collapse of rotating stars lead to much weaker convection and, as we shall see in §5, weaker explosions.

Rotation further weakens the explosion because the angular momentum profile is stable to convection and constrains convection to the polar regions. This can be understood physically by estimating the change of force on a blob of material as it is slightly raised from a position r with density (ρ), angular momentum (j) and pressure (P) to a position $r + \Delta r$ with its corresponding density, angular momentum, and pressure ($\rho + \Delta\rho, j + \Delta j, P + \Delta P$). If the blob is allowed to reach pressure equilibrium in its new surroundings, the acceleration that it feels without rotation is simply: $\Delta a = \Delta a_{\text{buo}} = g(1 - (\rho + \Delta\rho)/\rho_{\text{blob}})$ where g is the gravitational acceleration and ρ_{blob} is the density of the blob of material after it has expanded/contracted to reach pressure equilibrium. If the change in acceleration is positive, the blob of material will continue to rise and that region is convectively unstable. This gives us the standard Schwarzschild/Ledoux instability criteria (Ledoux 1947): a region is unstable if $(\partial\rho/\partial r) < (\partial\rho/\partial r)_{\text{adiabat}}$, or, for constant composition, $\partial S/\partial r > 0$. If there is an angular momentum gradient, however, the net force on the blob becomes:

$$\Delta a = g \left(1 - \frac{\rho + \Delta\rho}{\rho_{\text{blob}}} \right) + \frac{j_{\text{blob}}^2 - (j + \Delta j)^2}{(r + \Delta r)^3} \quad (2)$$

where $j_{\text{blob}} = j$. The corresponding Solberg-Høiland instability criterion is (Endal & Sofia 1978):

$$\frac{g}{\rho} \left[\left(\frac{d\rho}{dr} \right)_{\text{adiabat}} - \frac{d\rho}{dr} \right] > \frac{1}{r^3} \frac{dj^2}{dr} \quad (3)$$

If the angular momentum increases with increasing radius as it does for our core collapse models (Fig. 8), then the entropy gradient must overcome the angular momentum gradient to drive convection. In our simulations, the high entropy bubbles are unable to rise through the large angular momentum gradient and the convection is constrained to the polar region. The overwhelming effect of rotation on supernova models is this constraint on the convection and it causes weaker, asymmetric explosions.

5. Explosions And Compact Remnants

Because the convection is limited in rotating models, the convective region has less energy and is unable to overcome the pressure at the accretion shock as early as the non-rotating models which explode within 200 ms of bounce. However, at later times (500 ms after bounce) when the density of the infalling material decreases, the rotating models are able to launch an explosion, but the explosion occurs later and the proto-neutron star accretes slightly more mass (Fig. 9, Table 2). The final compact remnant mass, however, depends upon the amount of material that falls back onto the proto-neutron star. By

mapping our explosions back into one-dimension, we can estimate the amount of fallback and the observed explosion energy (Table 2). The masses in Table 2 are baryonic masses and the gravitational masses, which can be compared to observations, are typically $\sim 10\%$ lower. Mass estimates from observations of close binaries predict gravitational masses for stars without hydrogen envelopes to be $\sim 1.4 M_{\odot}$. Even including fallback, our non-rotating models produce remnants with masses which are much lower than those observed. Although the remnant masses of rotating models match observations much better, the explosion energies are too low to explain all the observations. Due to the uncertainties in other aspects of the supernova simulation (e.g., neutrino physics), we can not claim that rotating stars are required to make close compact binaries or that non-rotating stars are required to explain most supernova observations. But we can be reasonably sure of the trends: rotating stars produce weaker explosions and more massive remnants. As a further consequence, the rotating stars eject notably less ^{56}Ni (Table 2), up to one half for some of our explosions.

Not only are the explosions weaker for rotating stars, but since the convection is constrained to the poles, the explosion is stronger along the poles (Figures 10, 11). At the end of the simulation, ~ 1.5 s after bounce, the shock radius is 1.4 times further out along the pole than along the equator for our rotating star (Table 2). The mean velocity of the shocked material being ejected at the end of the simulation (2/3 of the explosion energy is still thermal) is $13,000 \text{ km s}^{-1}$ along the pole and only $5,100 \text{ km s}^{-1}$ along the equator! The maximum velocity along the pole can be as high as $18,000 \text{ km s}^{-1}$. These results must be taken with some degree of caution, since the axis of symmetry lies along the polar axis, and some of this asymmetry could be due to numerical artifacts. However, if we compare these results with a non-rotating star, we are encouraged that this asymmetry is real. In the case of a non-rotating star, the shock radius is only 4% further out along the poles, and the mean polar, equatorial velocities are $8,000 \text{ km s}^{-1}$, $7,700 \text{ km s}^{-1}$ respectively (maximum velocities are as high as $20,000 \text{ km s}^{-1}$). The variations from pole to equator in the non-rotating simulations are likely to be caused by the position of the rising bubbles and down-flows during the explosion. Even if these variations were all due to numerical artifacts (it could be due to convection plumes and hence, physical), it appears that numerical artifacts can account for only 10% variations in the velocities and the large asymmetry in the rotating simulations are likely to be real. By constraining the convection to the poles, rotating models produce more than a factor of 2 asymmetry in the explosion.

Neutrino luminosities for rotating and non-rotating stars are plotted in figure 12. The non-rotating core has a much larger μ and τ (ν_x) neutrino luminosity, especially just after bounce. This is because the non-rotating core compresses more and, at the μ and τ neutrinosphere, the temperature is over a factor of 1.5 higher than that of the rotating core. The large dependence of neutrino emission on temperature (the luminosity from pair annihilation $\propto T^9$), causes this small change in temperature to have large effects on the neutrino luminosity. Also, bear in mind that beyond 0.2s after bounce, the convective regions in the star look dramatically different. The non-rotating star has already launched an explosion, leaving a hot, bare proto-neutron star which continues to cool by emitting neutrinos. The rotating core is still convecting, and its neutrinosphere is further out. These differences are more easily seen in a plot of neutrino energies (Fig. 13). We infer no net asymmetry in the neutrino luminosity. But because of our coarse resolution, and the rapid time variation of the neutrino luminosity as bubbles rise above the neutrinosphere, asymmetries of $\sim 20 - 30\%$ could be hidden in our data and we can neither confirm nor rule out the asymmetric neutrino emission seen by Janka & Mönchmeyer (1989).

Rotating progenitors produce rotating compact remnants. Table 2 lists the spin period of the compact remnant assuming solid body rotation both at the end of the simulation before the neutron star has cooled and after it has cooled to a 10km neutron star. Even for Model 3 (Fig. 8, Table 2), which includes the

transport of angular momentum using an α -disk prescription, at the end of the simulation, the angular momentum in the proto-neutron star is sufficient to produce a ms pulsar. This is because, at the end of our SPH simulations, the proto-neutron star is still large, and it is not rotating rapidly. Hence, viscous momentum transport does not have an opportunity to remove the angular momentum from the core. As the neutron star contracts and the spin increases, the neutron star will lose angular momentum through a wind. Hence, the spin period of the cooled neutron star should be seen as a lower limit. In addition, convection in the cooling proto-neutron star (Burrows, Mazurek, & Lattimer 1981; Keil, Janka, & Müller 1996) will increase the efficiency of the viscous transport of angular momentum. Even in the absence of any wind, gravitational radiation limits the spin period to ~ 3 ms (Lindblom, Mendell, & Owen 1999). fallback may be able to spin up the neutron star, but will not be able to exceed the limit from gravitational radiation because the accreting material heats the neutron star to temperatures where gravitational radiation will effectively remove the angular momentum (Fryer, Colgate, & Pinto 1999).

A common problem to all core-collapse simulations which produce explosions is the large amount of neutron rich ejecta. Although the amount of material ejected with extremely low electron fraction ($Y_e < 0.4$) decreases from $1.2 \times 10^{-3} M_\odot$ for the non-rotating model to $1.1 \times 10^{-5} M_\odot$ for the rotating case, but due to the delayed explosion which gives more time for neutrino emission to deleptonize the ejecta, the amount of mildly neutron rich material ($Y_e < 0.49$) actually increases: 0.36, 0.60 M_\odot respectively for the non-rotating, rotating models. The material which falls back onto the neutron star will be mostly comprised of this neutron rich material. However, even assuming only neutron rich material falls back onto the neutron star, $> 0.1 M_\odot$ of neutron rich material is ejected, several orders of magnitude greater than the $10^{-2} - 10^{-3} M_\odot$ constraint from nucleosynthesis (Trimble 1991). Clearly, the delayed explosion caused by rotating does not solve the nucleosynthesis problem of the current exploding core-collapse models.

6. Implications

Rotation limits the convection in core-collapse supernovae, both by weakening the shock and by constraining the convection to the polar regions. Because of these constraints, the convective region takes longer to overcome the accretion shock and the explosion occurs at later times and is less energetic. The resultant compact remnants of the collapse of rotating stars are more massive. For higher mass progenitors, the density of the infalling material, and hence the shock pressure, increases (Burrows & Goshy 1993). Because of their limited convection, rotating cores are less likely to overcome the accretion shock, and the critical mass limits for black hole formation (both from fallback and direct collapse) are likely to be lower than those predicted for non-rotating stars (see Fryer 1999). Hence, the same rotation required to power a collapsar (MacFadyen & Woosley 1999) also causes the supernova to fail and the formation of a black hole. We expect a range of progenitor mass limits for black hole formation depending on the core rotation. This may help to explain the observed range of black hole systems (Ergma & van den Heuvel 1998). We stress that the uncertainties in the numerical implementation of the physics (e.g., neutrino transport, neutrino cross-sections, equation of state, symmetric gravity) limit our ability to make quantitative estimates, and the numbers should be regarded merely as “best-estimates”. The trends (e.g., weaker explosions, lower black hole formation limits) are more secure.

If angular momentum were conserved, the rotation periods of neutron stars formed from our progenitor model would be much faster than that expected in nascent neutron stars. However, winds and gravitational radiation will remove much of the angular momentum. If anything, it will be difficult to explain any rapidly spinning nascent neutron stars.

Not only are the explosions of rotating core-collapses weaker, but they are highly asymmetric (roughly a factor of 2 in the mean velocities from pole to equator). Polarization measurements of core-collapse supernova suggest that most supernovae are polarized (Wang et al. 1996; Wang & Wheeler 1998). In modeling Supernova 1993J, Höflich et al. (1995) required explosions with asymmetries of a factor of 2, roughly the same asymmetry we see in our simulations, and hence, rotation provides a simple explanation of polarization measurements. These asymmetric explosions also provide a simple explanation for the extended mixing in supernovae. Observations of Supernova 1987A in the X-rays (Dotani et al. 1987, Sunyaev et al. 1987), γ -rays (Matz et al. 1988), and even in the infra-red (Spyromilio, Meikle, & Allen 1990) all push toward extended mixing of iron-peak elements. The matter ejected along the poles, with their much higher velocities, will mix deeper into the star. To quantitatively determine the amount of mixing and polarization produced by the asymmetric explosions of our rotating cores, multi-dimensional simulations must be run out to late times.

We do not model magnetic fields in our simulations, but we can place some constraints on their importance in the supernova explosion. Thompson & Duncan (1993) have argued against primordial magnetic fields for neutron stars and, instead, suggest that strong neutron star magnetic fields are produced in dynamos during the supernova explosion itself. They propose a high Rossby number ($Ro = P_{\text{rot}}/\tau_{\text{con}}$ where P_{rot} is the rotation period and τ_{con} is the convective turnover timescale) dynamo, which takes advantage of the fast convection velocities, and hence high Rossby numbers, of core-collapse supernovae. However, this dynamo requires many convective turnovers ($\tau_{\text{con}} \lesssim 10^{-3} T_{\text{exp}}$, where T_{exp} is the explosion time) to significantly magnify the magnetic fields. Unfortunately, for our rotating supernovae, with typical convection length scales and velocities of ~ 400 km, ~ 4000 km s $^{-1}$ respectively, the explosion is launched before convection can produce a strong magnetic field. In addition, until the proto-neutron star cools and contracts, the rotation period of the disk-like structure is also slow (Table 2), and a rotation driven dynamo will not occur until after the supernova explosion.

As the proto-neutron star cools and shrinks, however, the Thompson & Duncan (1993) dynamo, driven by Ledoux convection (see Burrows, Mazurek, & Lattimer 1981; Keil, Janka, & Müller 1996) is more promising. The strength of this convection is still a matter of debate (Mezzacappa et al. 1998b), but if it is as strong as Keil, Janka, & Müller (1996) predict, magnetic fields in excess of 10^{15} G are obtainable at late times using the convection-driven dynamo of Thompson & Duncan (1993). These magnetic fields will enhance the angular momentum lost in the proto-neutron star wind. But in all of our simulations, this occurs after the launch of the explosion, and the magnetic field would not affect the supernova explosion.

Lastly, and most speculatively, we come to the topic of neutron star kicks. There is a growing set of evidence that neutron stars are born with high space velocities with a mean magnitude ~ 450 km s $^{-1}$ (see Fryer & Kalogera 1998 for a review). Rotation breaks one symmetry, and it is tempting to speculate that it is then easy to break an additional symmetry causing a net momentum in the ejecta which is non-zero. To balance out the momentum, the neutron star must then have gained some momentum. Indeed, the net momentum of the ejecta along the poles in our simulation is 6×10^{39} g cm s $^{-1}$. This corresponds to a kick velocity of only 30 km s $^{-1}$, over an order of magnitude too small to explain the observed pulsar velocity distribution. And this momentum may be entirely a numerical artifact. Asymmetric neutrino emission can also cause neutron star kicks, but we detect no significant neutrino asymmetry. In any event, calculating quantitative results on neutron star kicks requires 3-dimensional simulations where a fixed inner boundary is not necessary and the proto-neutron star is allowed to move.

This research has been supported by NASA (NAG5-2843, MIT SC A292701, and NAG5-8128), the NSF

(AST-97-31569), the US DOE ASCI Program (W-7405-ENG-48), and the Alexander von Humboldt-Stiftung (FLF-1065004). It is a pleasure to thank Stan Woosley, Andrew MacFadyen and Norbert Langer for encouragement and advice.

REFERENCES

- Bodenheimer, P., & Woosley, S.E., 1983, ApJ, 269, 281
- Bonazzola, S. & Marck, J.A., 1993, A&A, 267, 623
- Burrows, A., Mazurek, T. J., & Lattimer, J. M. 1981, ApJ, 251, 325
- Burrows, A., & Goshy, J. 1993, ApJ, 416, L75
- Burrows, A., Hayes, J., & Fryxell, B. A. 1995, ApJ, 450, 830
- Chaboyer, B. & Zahn, J.-P. 1992, A&A, 253, 173
- Colgate, S.A. & White, R.H., 1966, ApJ, 143, 626
- Dotani, t., et al. 1987, Nature, 330, 230
- Endal, A. S., Sofia, s. 1978, ApJ, 220, 279
- Ergma, E. & van den Heuvel, E. P. J. 1998, A&A, 331, L29
- Finn, L.S. & Evans, C.R., 1990, ApJ, 351, 588
- Fryer, C. L., & Kalogera, V. 1998, ApJ, 489, 244
- Fryer, C. L., 1999, accepted by ApJ
- Fryer, C. L., Herant, M., Benz, W., Colgate, S. A., 1999, accepted by ApJ
- Fryer, C. L., Colgate, S. A., & Pinto, P. A. 1999, ApJ, 511, 885
- Fukuda, I. 1982, PASP, 94, 271
- Grevesse, N., Noels, A. 1993, in Origin and Evolution of the Elements, eds. N. Prantzos, E. Vangioni-Flam, M. Casse, Cambridge: Cambridge University Press, p. 13
- Heger, A. 1998, PhD Thesis, Technische Universität München
- Heger, A., Langer, N., & Woosley, S. E. 1999, ApJ, accepted.
- Herant, M., Benz, W., Hix, W. R., Fryer, C. L., Colgate, S. A. 1994, ApJ, 435, 339
- Höflich, P., Wheeler, J. C., Hines, D., Trammell, S. 1995, ApJ, 459, 307
- Janka, H.-T. & Mönchmeyer, R., 1989, A&A, 209, L5
- Janka, H.-T., Zwerger, T., & Mönchmeyer, R., 1993, A&A, 268, 360
- Janka, H.-T. & Müller, E. 1996, A&A, 306, 167

- Keil, W., Janka, H.-T., & Müller, E. 1996, *ApJ*, 473, L111
- LeBlanc, J.M. & Wilson, J.R., 1970, *ApJ*, 161, 541
- Ledoux P., 1947, *ApJ*, 105, 305
- Lindblom, L., Mendell, G., & Owen, B. J. 1999, gr-qc/9902052
- Livio, M., Pringle, J. E. 1998, *ApJ*, 505, 339
- MacFadyen, A. & Woosley, S. E. 1999, accepted by *ApJ*
- Marshall, F. E., Gotthelf, E. V., Zhang, W., Middledich, J., & Wang, Q. D. 1998, *ApJ*, 499, L179
- Matz, S. M., et al. 1988, *Nature*, 331, 416
- Messer, O. E. B., Mezzacappa, A., Bruenn, S. W., & Guidry, M. W. 1998, *ApJ*, 507, 353
- Mezzacappa, A., Calder, A. C., Bruenn, S. W., Blondin, J. M., Guidry, M. W., Strayer, M. R., & Umar, A. S. 1998, *ApJ*, 495, 911
- Mezzacappa, A., Calder, A. C., Bruenn, S. W., Blondin, J. M., Guidry, M. W., Strayer, M. R., & Umar, A. S. 1998, *ApJ*, 493, 848
- Miller, D. S., Wilson, J. R., & Mayle, R. W. 1993, *ApJ*, 415, 278
- Mönchmeyer, R. & Müller, E., 1989, in NATO ASI series, Timing Neutron Stars, ed. H. Ögelman & E.P.J. van den Heuvel (New York: ASI)
- Mönchmeyer, R., Schäfer, G., Müller, E., Kates, R.E., 1991, *A&A*, 246, 417
- Müller, E., Rożyczka, M., & Hillebrandt, W., 1980, *A&A*, 81, 288
- Müller, E. & Hillebrandt, W., 1981, *A&A*, 103, 358
- Pinsonneault, M. H., Kawaler, S. D., Sophia, S., Demarque, P. 1989, *ApJ*, 338, 424
- Rampp, M., Müller, E., & Ruffert, M., 1998, *A&A*, 332, 969
- Shakura, N. I., Sunyaev, R. I. 1973, *A&A*, 88, 23
- Spruit, H. C. 1998, *A&A*, 333, 603
- Spruit, H. C., & Phinney, E. S. 1998, *Nature*, 393, 193
- Spyromilio, J., Meikle, W. P. S., & Allen, D. A. 1990, *MNRAS*, 242, 669
- Sunyaev, R., et al. 1987, *Nature*, 330, 227
- Symbalisty, E.M., 1984, *ApJ*, 285, 729
- Tassoul, J. L. 1978, *Theory of Rotating Stars*, ed. J. Ostriker, university Press (Princeton)
- Tohline, J.E., Schombert, J.M., & Boss, A.P., 1980, *Space Science Review*, 27, 555
- Trimble, V. 1991, *A&A Rv.*, 3, 1

- Wang, L., Wheeler, J. C., Li, Z. W., & Clocchiatti, A. 1996, *ApJ*, 467, 435
- Wang, L., & Wheeler, J. C. 1999, *ApJL*, in press
- Wilson, J. R., & Mayle, R. W. 1988, *Phys. Rep.*, 163, 63
- Woosley, S. E., & Weaver, T. A. 1995, *ApJS*, 101, 181
- Weaver, T. A., Zimmermann, G. B., & Woosley, S. E. 1978, *ApJ*, 225, 1021
- Yamada, S., & Sato, K., 1995, *ApJ*, 434, 268
- Yamada, S., & Sato, K., 1995, *ApJ*, 450, 245
- Zahn, J.-P. 1975, *Mem. Soc. Roy. Sci. Liège*, 8, 31
- Zahn, J.-P. 1992, *A&A*, 265, 115.
- Zwinger, T. & Müller, E., 1997, *A&A*, 320, 209

Table 1. Rotating Models

Model Number	Angular Momentum	M_{core} (M_{\odot})
1	$J_{\text{Heger}}(r)$	0.05
2	$J_{\text{Heger}}(r)$	0.09
3 ^a	$J_{\text{Heger}}(r)$	0.05
4 ^b	$J_{\text{Heger}}(r)$	0.05
5	$0.5 \times J_{\text{Heger}}(r)$	0.05
6	0.	0.05
7	0.	0.09
8 ^c	0.	0.01

^aHigh resolution run $\sim 32,000$ particles

^bThis model includes an α -disk prescription for the artificial viscosity with α_d set to 0.1 (§3).

^cThis simulation uses the progenitor model s15s7b from Woosley & Weaver (1995). All other simulations use the progenitor described in §2 (Heger 1998).

Table 2. Rotating Models

Model #	$T_{\text{exp}}^{\text{a}}$ s	$E_{\text{exp}}^{\text{b}}$ 10^{51} ergs	$M_{\text{rem}}^{\text{c}}$ M_{\odot}	Explosion Asymmetry $r_{\text{shock}}^{\text{pole}}/r_{\text{shock}}^{\text{equ}}$	$V_{\text{pole}}, V_{\text{equ}}$	Rotation ^d ms	Ejecta (M_{\odot}) ^e $Y_e < 0.49$	^{56}Ni
1	0.5	0.95,0.5	1.2,1.5	1.4	13,5.1	260,1.8	0.60,0.30	0.15
2	0.5	1.2,0.5	1.2,1.5	1.3	12,6.1	140,1.7	0.56,0.25	0.2
3 ^f	0.5	-	-	-	-	-	-	-
4	0.5	1.5,0.7	1.1,1.3	1.3	12,5.5	70,1.9	0.45,0.25	0.2
5	0.4	1.9,1.3	1.2,1.3	1.2	12,9.0	260,1.9	0.50,0.40	0.3
6	0.2	2.1,1.5	1.1,1.2	1.04	8.0,7.7	-	0.36,0.25	0.3
7	0.2	2.2,1.6	1.1,1.2	1.06	9.7,9.2	-	0.35,0.25	0.3
8	0.2	2.5,1.9	1.1,1.2	-	-	-	0.23,0.1	0.3

^aThe explosion time is the time from bounce until the shock has reached 2000 km.

^bThe explosion energy is given as both the net change in energy for the ejected material (see Fryer 1999) and the kinetic energy at infinity.

^cThe two values for remnant mass are before and after fallback.

^dThe rotation period of the neutron star at the end of the SPH simulation (when the star is still rather large) and after the neutron star has cooled assuming no angular momentum is lost.

^eThe first column gives the amount of neutron rich material ejected both before and after fallback. The second column gives the total nickel mass ejected.

^fWe have only run the high-resolution simulation to explosion (first ~ 0.5 s) and can not reliably estimate the explosion energy or amount of fallback. However, the explosion time and behavior agrees with the lower resolution runs.

Table 3. 1D explosion simulations

Model #	piston location M _⊙	piston alpha (art. part)	piston energy ^a 10 ⁵¹ ergs	art. pist. energy ^a 10 ⁵¹ ergs	explosion energy ^b M _⊙	fall back M _⊙	remnant mass M _⊙	⁵⁶ Ni ejected
1 ^c	1.10	0.0017	1.30	0.30	0.52	0.30	1.40	0.18
1	1.145	0.004	1.03	0.15	0.48	0.26	1.40	0.16
1	1.19	0.01	0.89	0.08	0.45	0.24	1.43	0.13
1	1.24	0.017	0.76	0.05	0.40	0.23	1.47	0.10
1	1.29	0.035	0.63	0.04	0.34	0.21	1.50	0.06
6	1.05	0.002	1.43	0.23	0.67	0.24	1.29	0.21
6	1.10	0.03	1.35	0.08	0.73	0.16	1.26	0.24
6	1.145	0.05	1.27	0.05	0.72	0.14	1.28	0.22
6	1.19	0.07	1.09	0.05	0.64	0.15	1.34	0.18
6	1.24	0.1	0.97	0.03	0.60	0.15	1.39	0.14
6	1.29	0.12	0.80	0.03	0.49	0.16	1.45	0.07
6 ^d	1.10	0.03	1.34	2.31	0.73	0.15	1.25	0.24
6 ^d	1.10	0.04	1.41	2.38	0.80	0.15	1.25	0.24
6 ^d	1.10	0.10	1.74	2.71	1.13	0.13	1.23	0.27
6 ^d	1.10	0.17	2.05	3.02	1.44	0.11	1.21	0.29
6 ^d	1.10	0.19	2.13	3.10	1.52	0.10	1.20	0.29

^aIntegrated work of the piston

^bKinetic energy (of the ejecta) at infinity (~ 1 yr after explosion)

^cat 18.5s after core collapse the innermost 0.2 M_⊙ above the piston were removed from the grid and the new piston radius (10⁹ cm) kept constant. The deviation in the piston energy due to this modification is $< 1\%$.

^dartificial piston is started when Lagrangian mass element reaches its minimum location

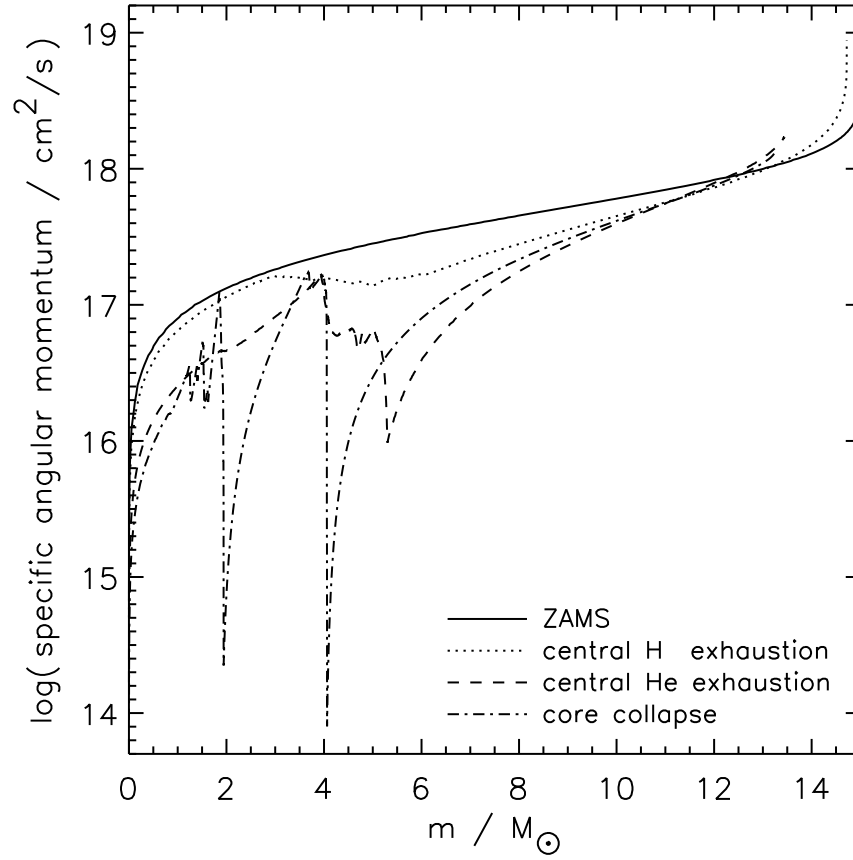


Fig. 1.— Specific angular momentum of the progenitor Model E15B at different evolutionary stages as a function of the interior mass coordinate. The profiles at core hydrogen ignition (ZAMS; solid line), central hydrogen depletion (dotted line), central helium depletion (dashed line), and at onset of core collapses (dash-dotted line) are given. See also Heger (1998); Heger, Langer & Woosley (1999).

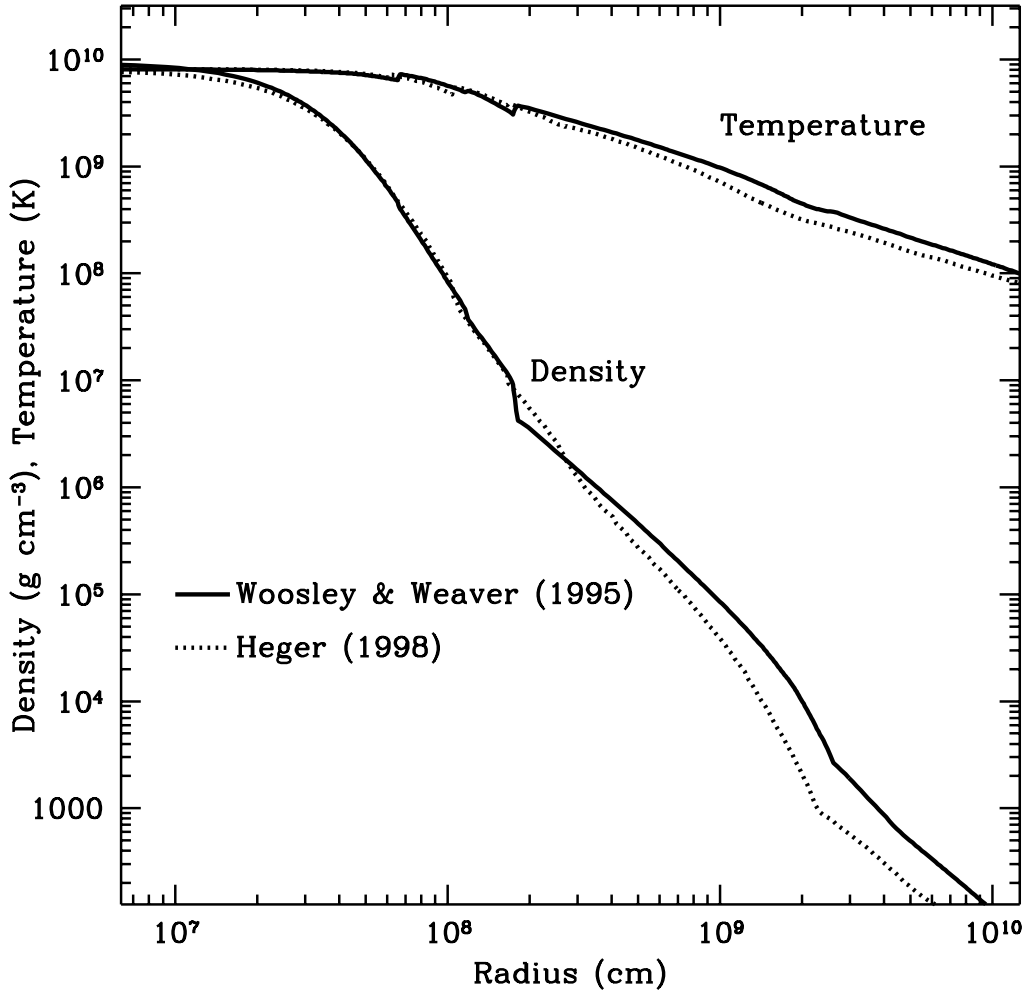


Fig. 2.— Density and Temperature profiles for our $15 M_{\odot}$ rotating progenitor (Heger 1998) and the Woosley & Weaver (1995) progenitor s15s7b. Beyond a radius of $3 \times 10^8 \text{ g cm}^{-3}$, the density of the rotating progenitor drops faster than s15s7b. Pressure equilibrium requires that the temperature decrease faster as well. Although this lower density makes it easier to drive a supernova explosion, its effect is small compared to the effects of rotation.

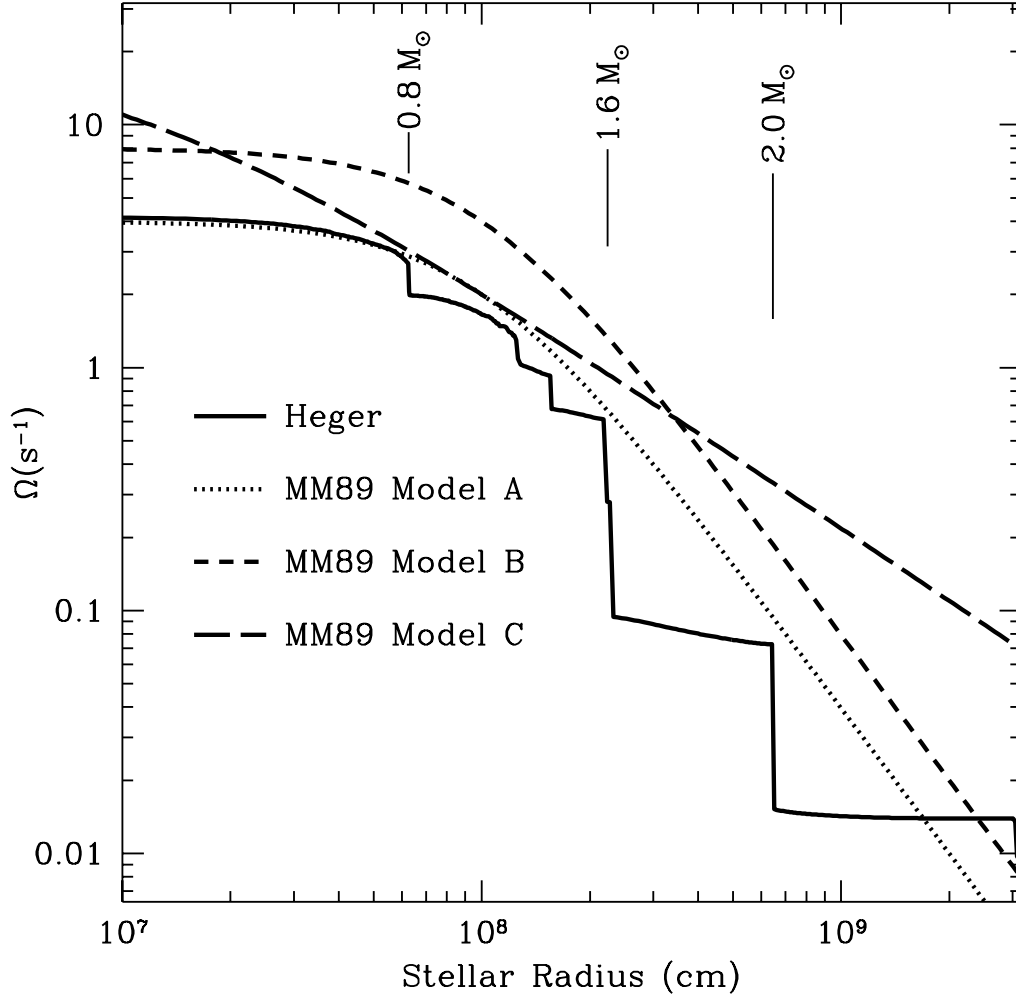
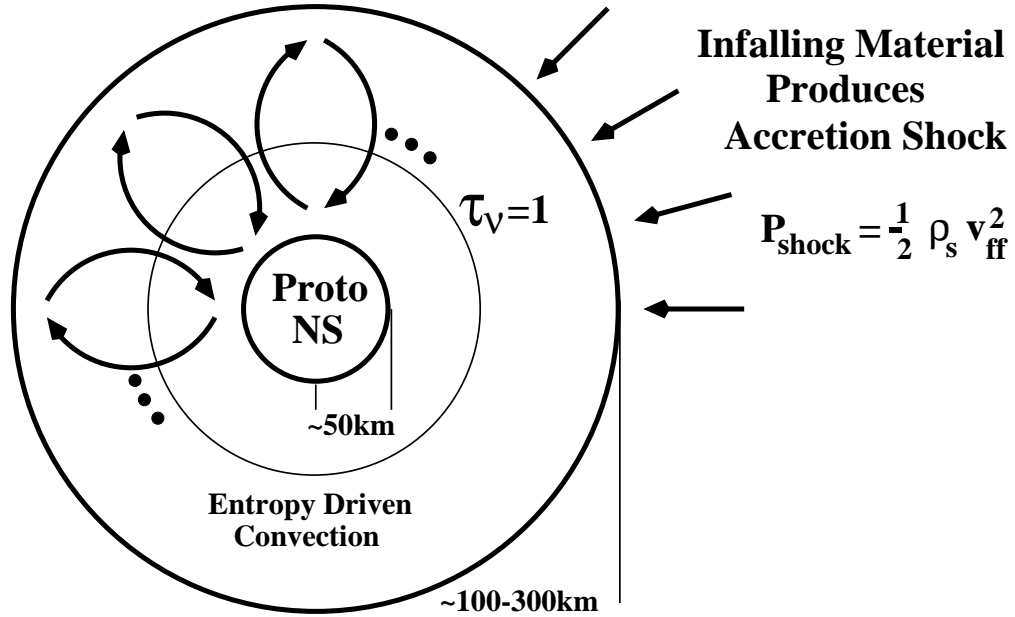


Fig. 3.— The angular velocity profile for our rotating model as well as the prescriptions used in the models of Mönchmeyer & Müller (1989). Except for model A, the models of Mönchmeyer & Müller (1989) are rotating more rapidly than our models and the effects of rotation on our collapse simulations are much less than most of their simulations. Also note that the angular velocity distribution is a series of step functions. This is because each convection region tends to equilibrate the angular velocity and only at convective boundaries does the angular velocity change significantly.

Spherically Symmetric Collapse



Rotating Collapse

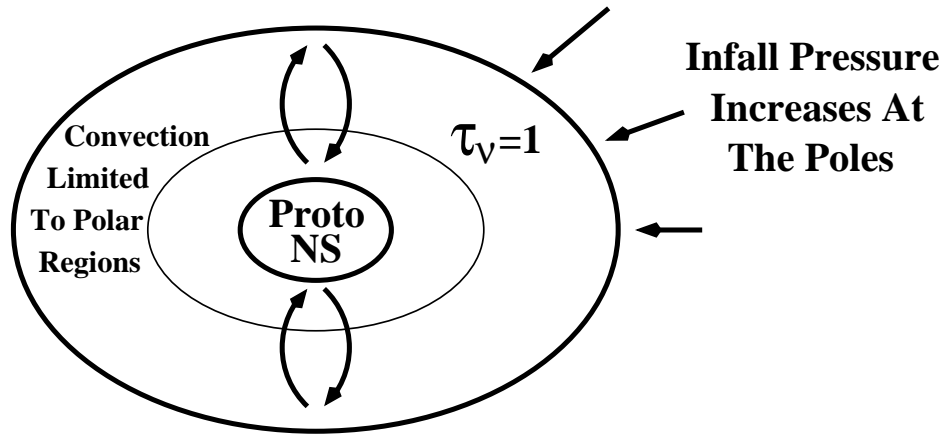


Fig. 4.— Entropy-driven convection has been found to enhance the energy deposition within the accretion shock. As the density of the infalling matter decreases, the convective region is able to push the shock outward, launching a supernova explosion. The proto-neutron star may also convect (Burrows, Mazurek, & Lattimer 1981; Keil, Janka, & Müller 1996), increasing the neutrino flux at its surface and the neutrino heating in the convective region. The angular momentum profile in rotating core-collapses stabilizes the convection along the equator.

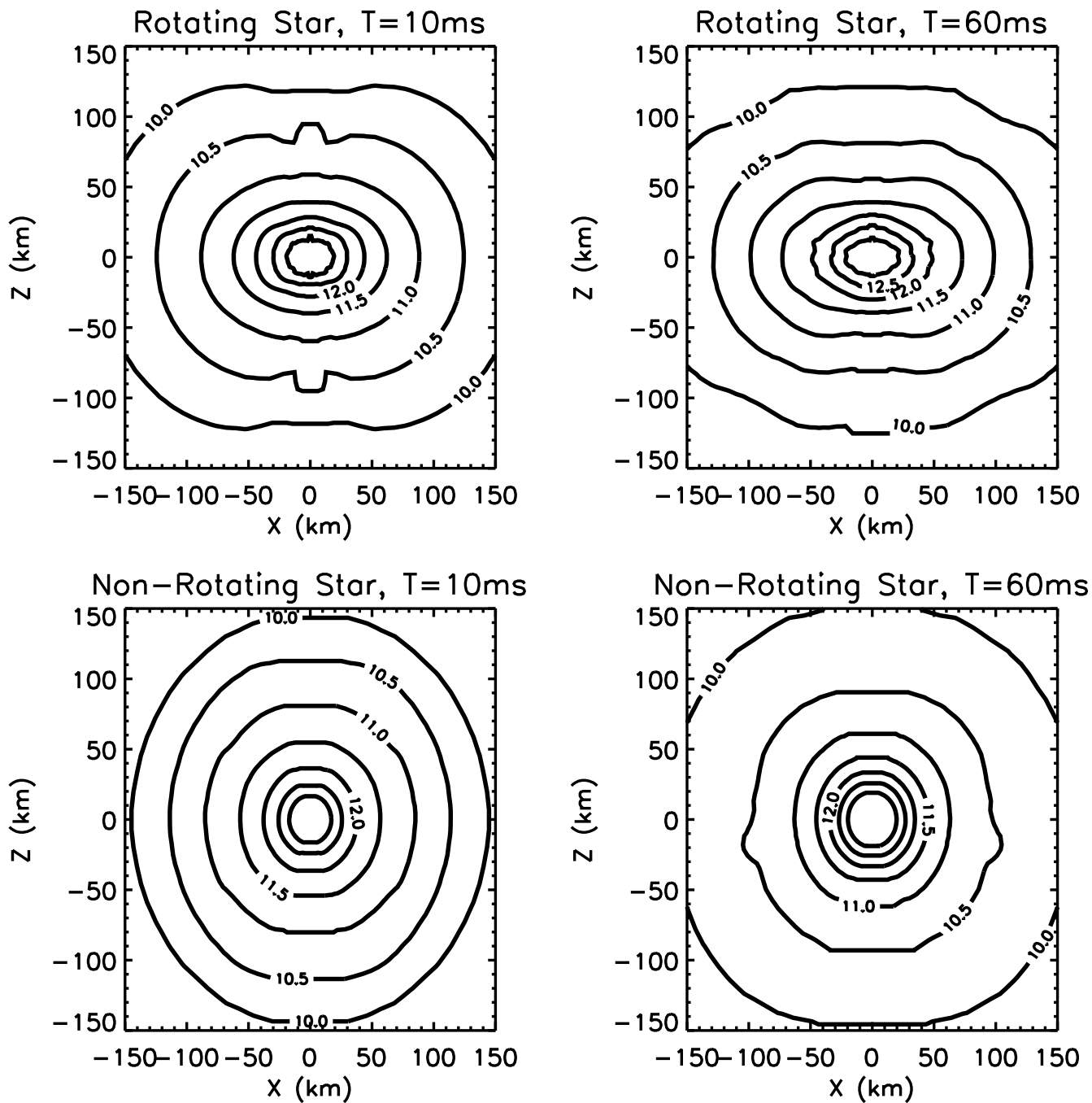


Fig. 5.— Surfaces of constant entropy (logarithmically spaced) for rotating and non-rotating stars (Models 1,5) at 10 and 60 ms after bounce. 60ms after the bounce, the axis ratio (pole/equator) of the proto-neutron star (densities $\gtrsim 10^{11} \text{ g cm}^{-3}$) has dropped to 0.6. At this time, the accretion shock of the rotating model is at $\sim 160, 300 \text{ km}$, respectively, for the poles, equator. In the case of a non-rotating star, the spherically symmetric accretion shock is at $\sim 300 \text{ km}$.

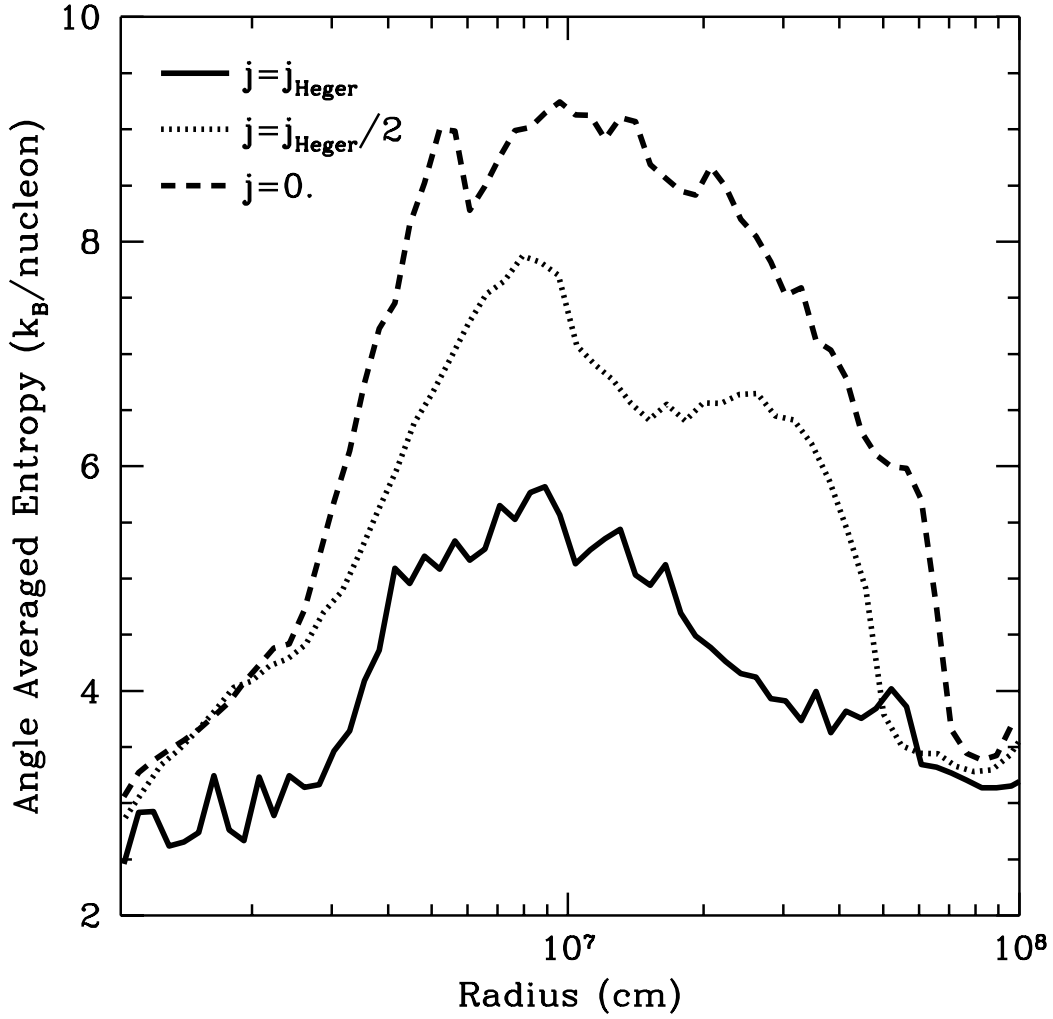


Fig. 6.— Angle-averaged entropy for stars with a range of initial angular momentum (Models 1,5,6). As the angular momentum increases, the entropy profile becomes shallower. The entropy gradient seeds the convection which must overcome the ram pressure of the accretion shock to produce a supernova explosion. Convection in the case of rotating stars will be less vigorous and these stars will explode later.

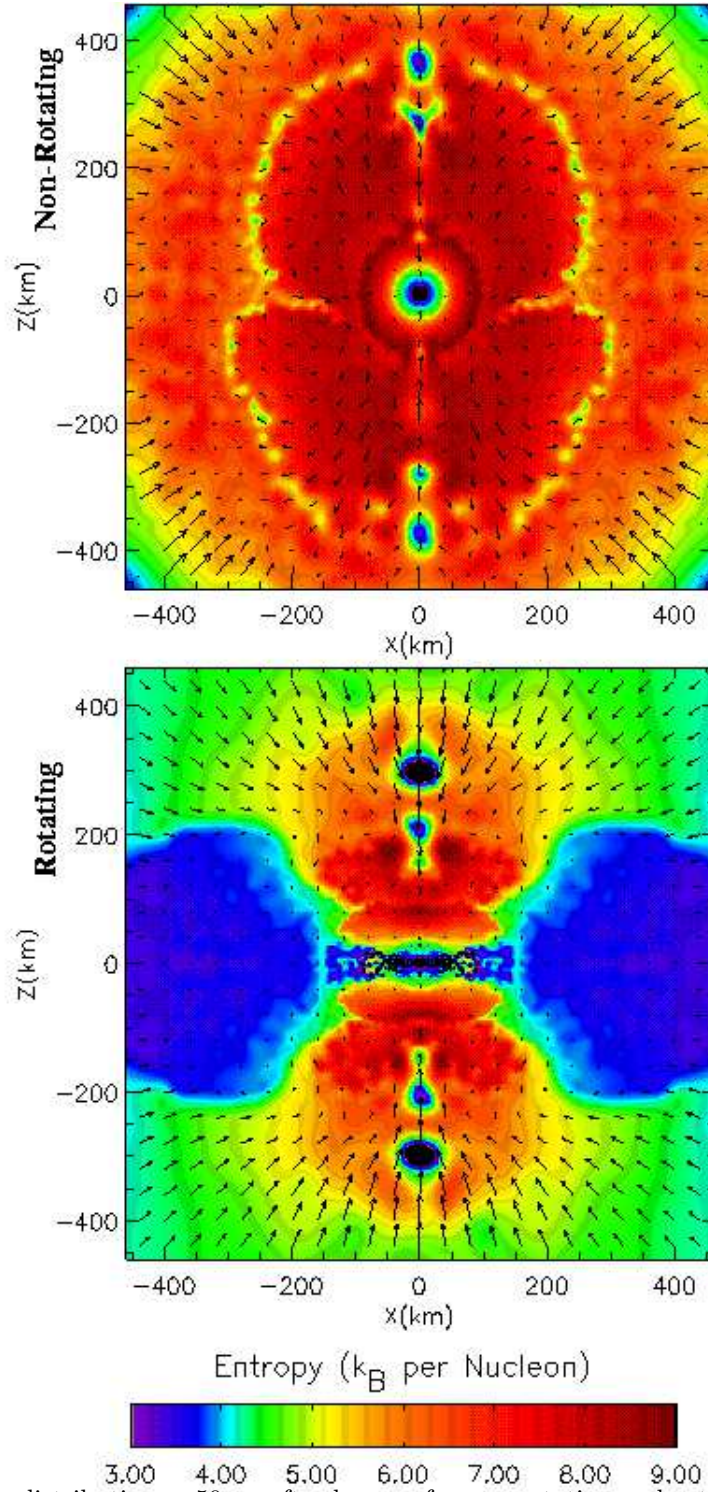


Fig. 7.— Entropy distribution ~ 50 ms after bounce for non-rotating and rotating cores. For the rotating model, the large increase in entropy caused by the bounce shock is limited to the polar region. The overlying velocity vectors show that the non-rotating model has already developed vigorous convection.

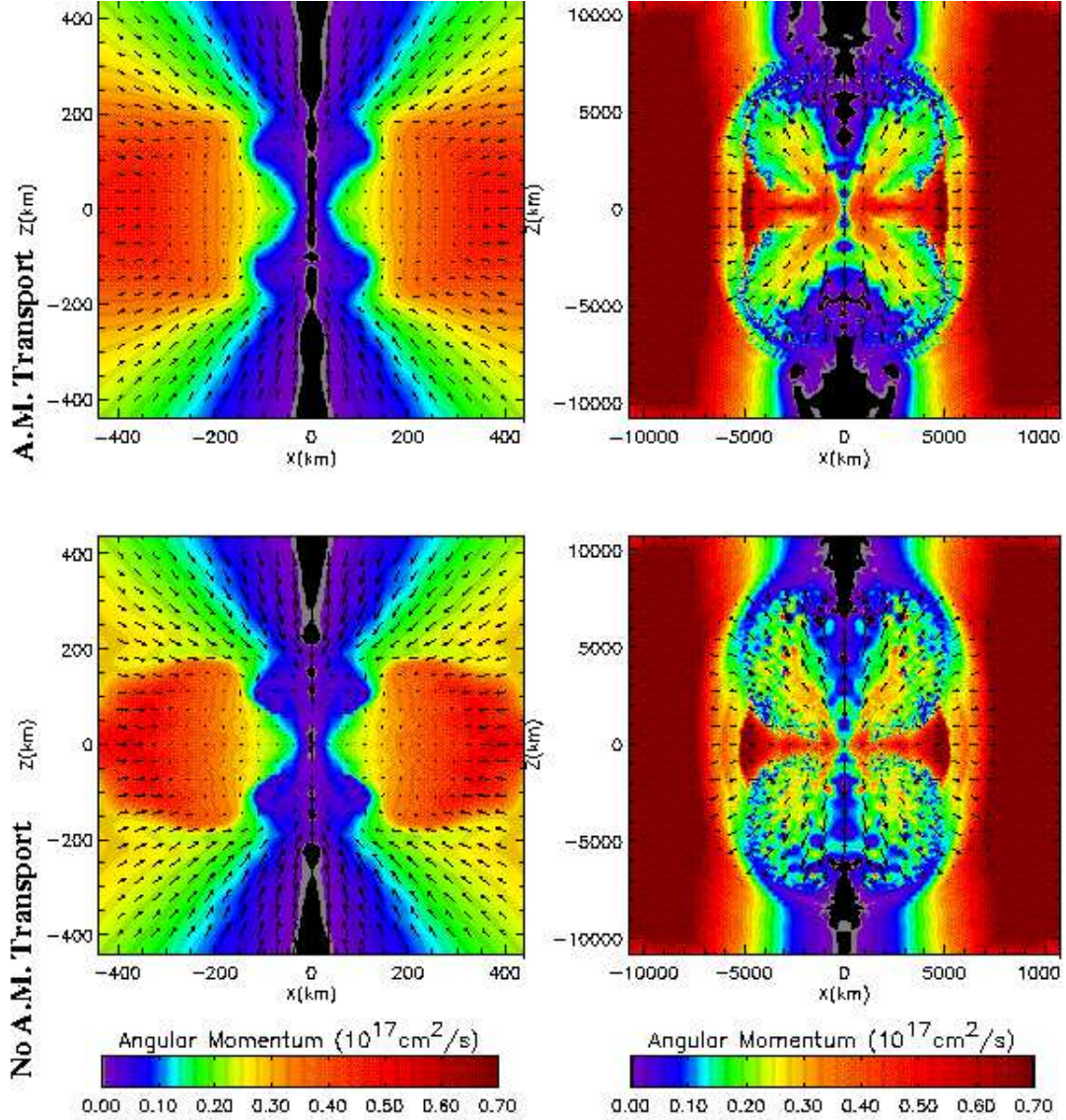


Fig. 8.— Angular momentum distribution roughly ~ 50 ms and at the end of the simulation for both Models 1 and 4. The large angular momentum gradient along the equator must be overcome to drive convection in the equatorial region. Angular momentum transport in Model 4 smooths the angular momentum profile, but because the rotation period is still roughly 0.1 s by the end of the simulation, the amount of angular momentum in the two models is similar. At late times, both models show the presence of a disk around the proto-neutron star.

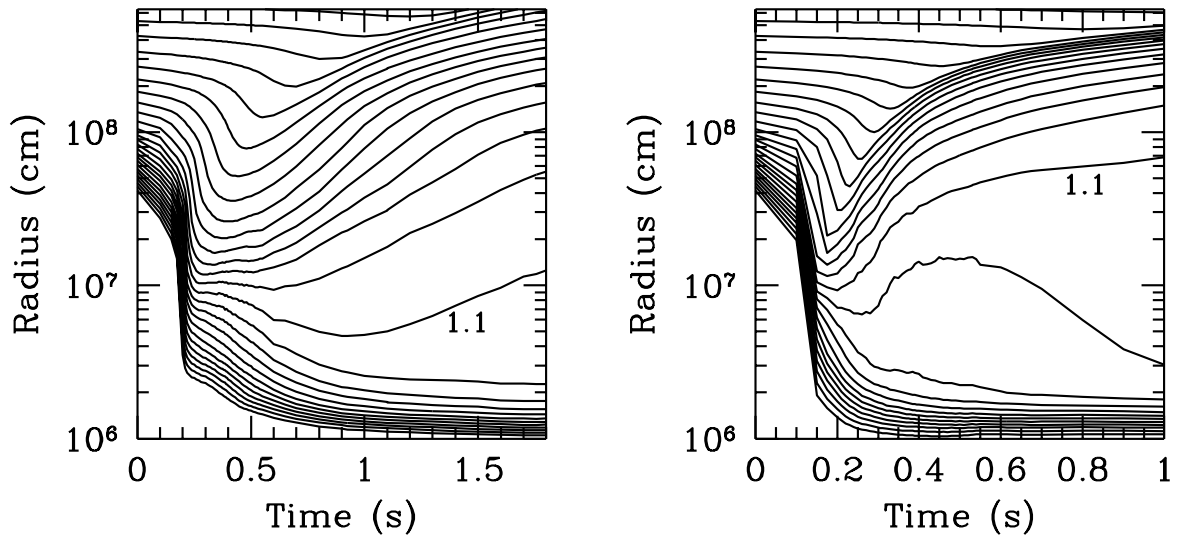


Fig. 9.— Mass trajectories vs. time for the rotating (left) and non-rotating (right) models (Models 1 and 6). Note that the rotating model explodes much later than the non-rotating case. The mass point which contains $1.1 M_{\odot}$ is labeled and every line demarks a change of $0.05 M_{\odot}$.

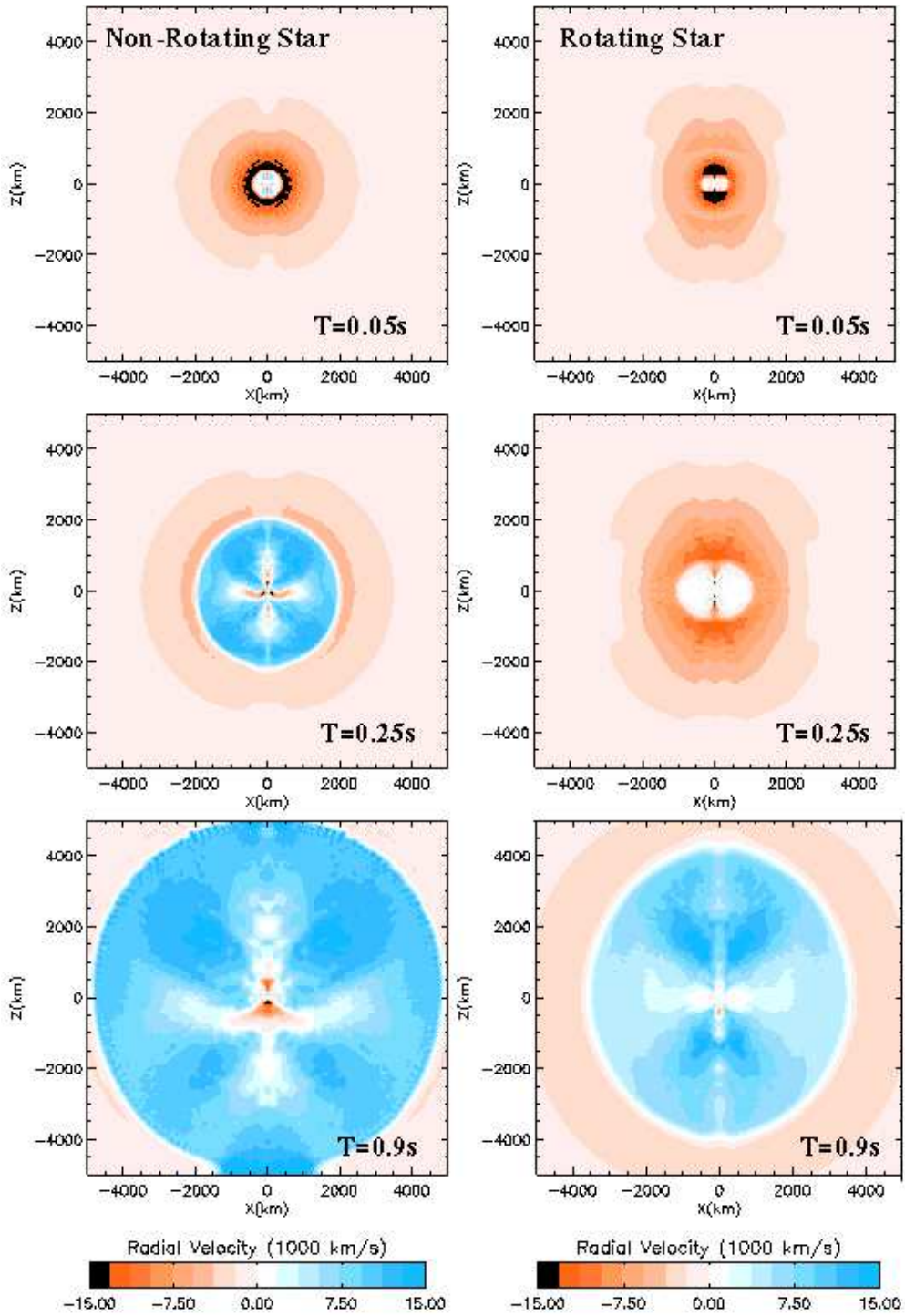


Fig. 10.— Radial velocity distribution of non-rotating and rotating models 0.05, 0.25, 0.5, and 0.9s after bounce. At 0.9s, the non-rotating model remains essentially spherical. The asymmetries in the velocities are caused by the buoyant convective bubbles which are driving the explosion. In contrast, the rotating model already shows strong asymmetries in the shock position and velocities.

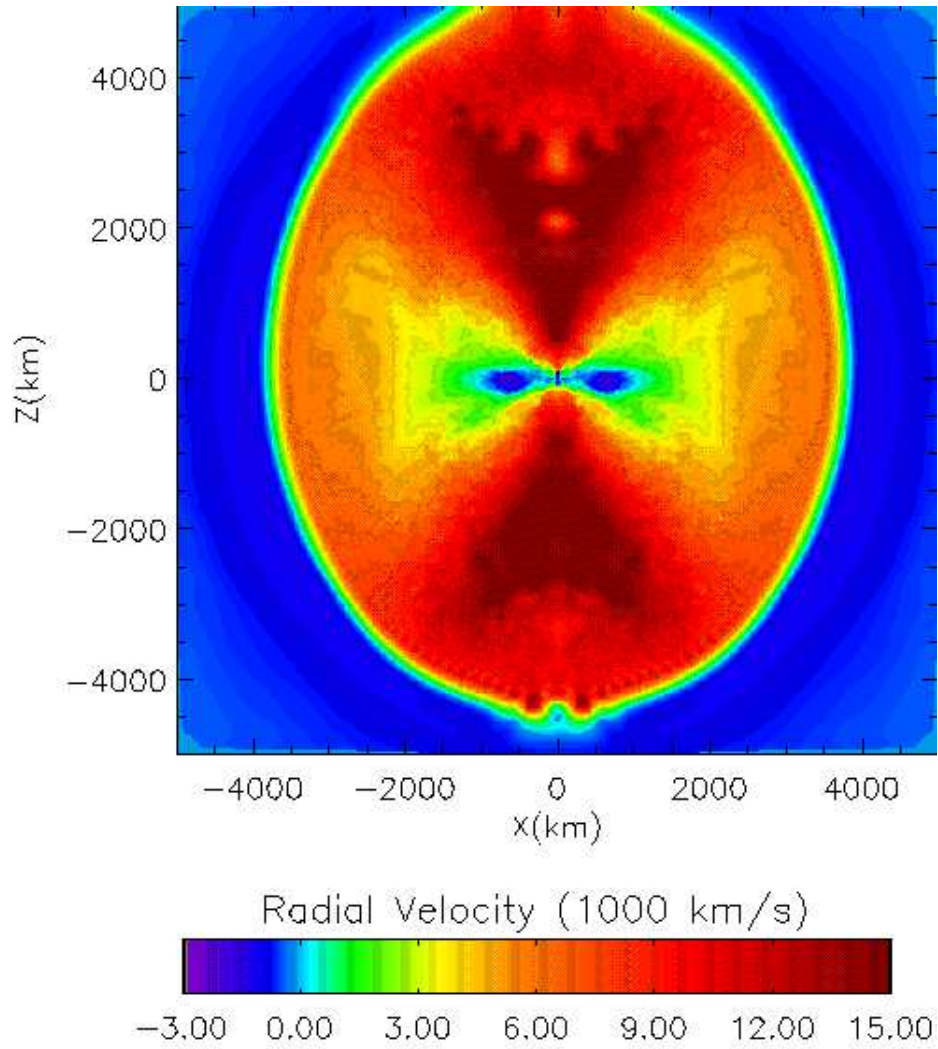


Fig. 11.— Radial velocity distribution of the non-rotating model (Model 1) 1.6s after bounce. Note the strong jet being driven in the polar region. The momentum asymmetry between the upper and lower pole is $6 \times 10^{39} \text{ g cm s}^{-1}$, which corresponds to a neutron star kick of roughly 30 km s^{-1} .

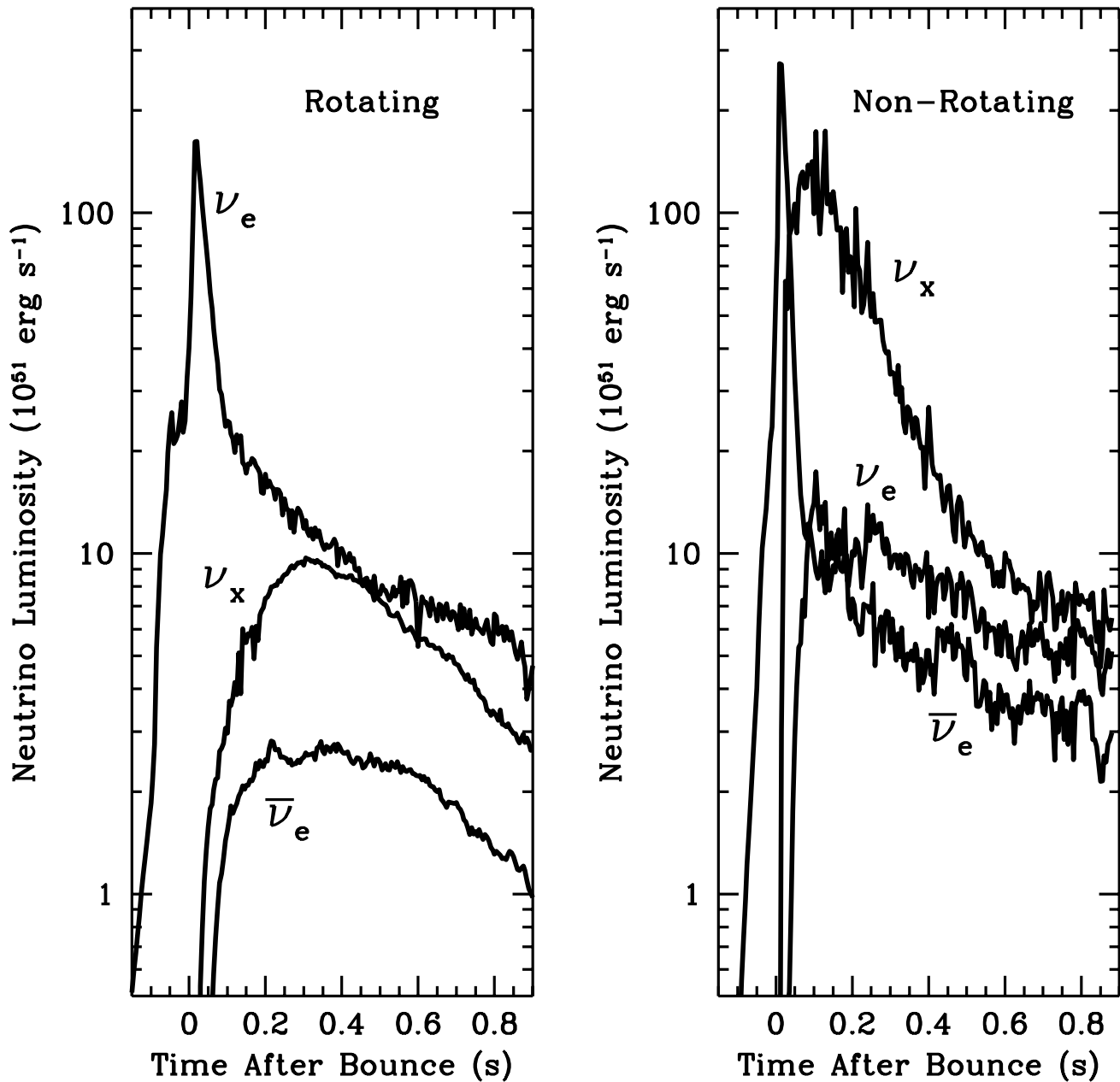


Fig. 12.— Neutrino luminosities versus time for a rotating and non-rotating progenitor (models 1 and 6). The non-rotating core has a much larger μ and τ (ν_x) neutrino luminosity, especially just after bounce. This is because the non-rotating core compresses more and, at the μ and τ neutrinosphere, the temperature is over a factor of 1.5 higher than that of the rotating core. Because of the large dependence of neutrino emission on temperature (the luminosity from pair annihilation $\propto T^9$), this small change in temperature has large effects on the neutrino luminosity.

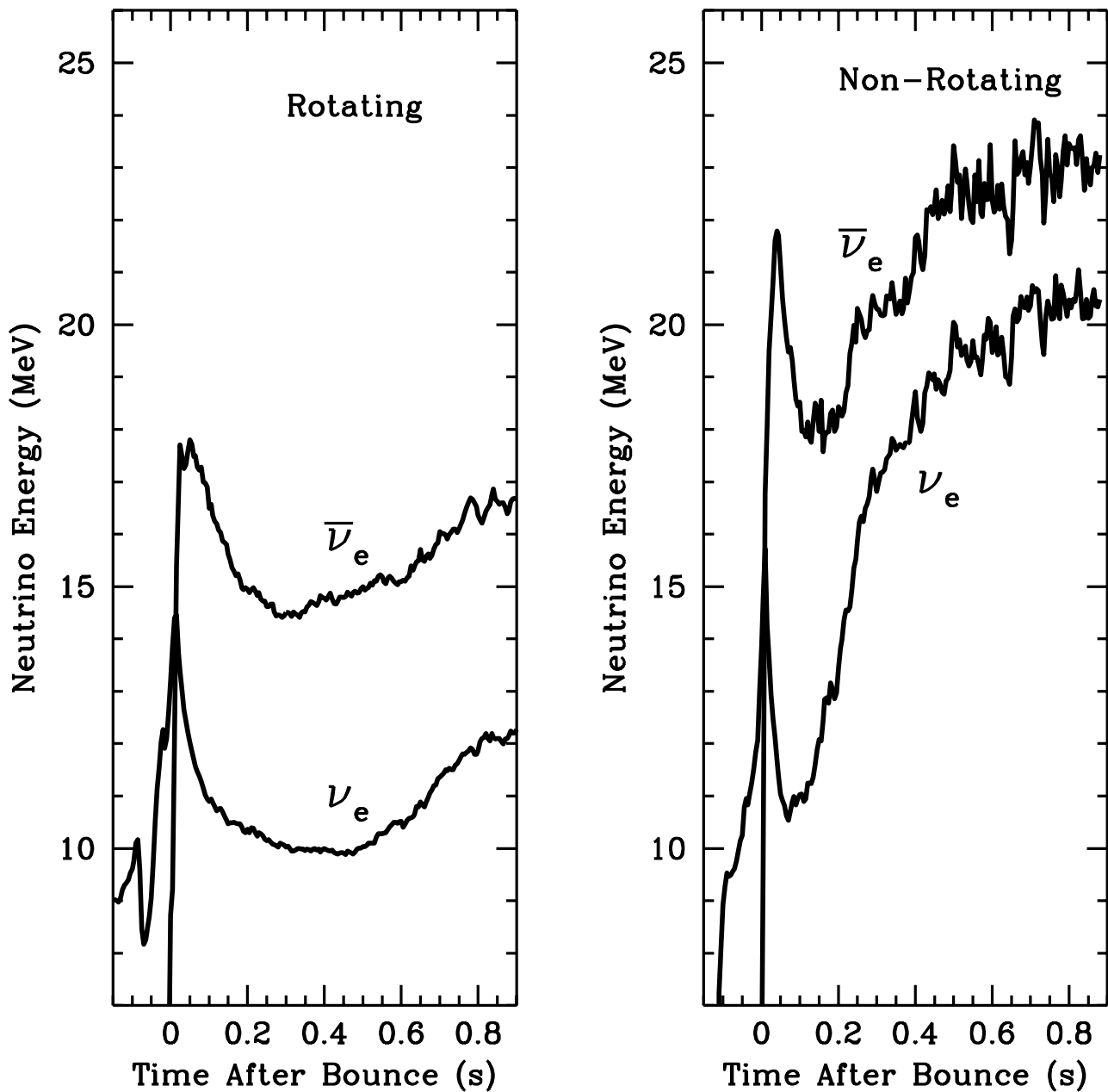


Fig. 13.— Electron and anti-electron neutrino energies versus time for a rotating and non-rotating progenitor (models 1 and 6). The neutrino energies for the non-rotating core at any given time after bounce are much higher. This is in part due to the larger compression, and hence higher temperatures of the non-rotating cores. But most of the difference can be explained by the explosion time. The non-rotating star explodes ~ 0.2 s after bounce, leaving a hot, bare proto-neutron star which continues to cool by emitting neutrinos. The rotating core is still convecting, and its neutrinosphere is further out where temperatures are lower.